Tellus (1994), 46A, 615–634
Printed in Belgium – all rights reserved

TELLUS
ISSN 0280–6495

Cloudiness parameterization and verification in a large-scale atmospheric model

By ASHU P. DASTOOR, *Recherche en Prévision Numérique, Service de l'Environnement Atmospherique, 2121, route Trans-Canadienne, Dorval, Quebec, Canada H9P 1J3*

(Manuscript received 13 May 1993; in final form 27 October 1993)

ABSTRACT

This paper addresses the problem of predicting cloud cover and its radiative impact in a large-scale atmospheric model. A convective and stratiform condensation scheme including cloud water content as a predictive variable is implemented in the Canadian global spectral model. An important aspect of the scheme is that the cloud amount estimation is a part of the condensation scheme and is a key element in the sub-grid scale stratiform condensation parameterization. The cloud cover from the scheme is verified quantitatively using satellite data. The dependence of the grid-scale relative humidity threshold on the horizontal and vertical resolutions is examined. The possibility of parameterizing stratiform clouds as vertically sub-grid clouds and its verification is investigated. It is shown that the total cloud cover is better estimated as the sum of separate estimates of convective and stratiform cloudiness within the framework of the condensation processes parameterized in the model. The convective cloud cover is found to be very important to the radiative budget. An improvement in the model forecast, hydrological balance and cloudiness prediction is noticed when the stratiform relative humidity threshold decreases with height. The study also presents a new 3-dimensional view of the cloudiness estimated by the original scheme and provides a simple vertical and horizontal sub-grid scale cloud cover parameterization. Vertically sub-grid stratiform clouds combined with horizontally sub-grid convective clouds provide a remarkable improvement in the estimation of total cloud cover.

1. Introduction

The planet Earth when visualized from space is seen to be dominated by clouds and their patterns. Cloudiness greatly complicates the dynamics of the atmosphere. The presence of clouds affects the atmospheric heating through reflection, absorption and emission of radiation, and the surface heat balance through modification of the solar and infrared fluxes reaching the ground. Changes in the distribution of cloudiness can, therefore, alter temperature gradients and vertical stability and thus affect circulation patterns. For over a decade, a number of observational and theoretical studies have established that clouds produce radiative heating and cooling effects that are comparable to the latent heating and fluctuate on dynamically active space and time scales (Albrecht and Cox, 1975; Stephens and Webster, 1979; Webster and Stephens, 1980; Ramanathan, 1987). On the inter-annual time scale, the interaction between cloud processes and radiative processes is of fundamental importance to the mechanisms of climatic change. Changes in the radiation balance at the top of the atmosphere are mainly controlled by the distribution of water in its various forms, which are water vapor and clouds of ice and/or liquid water. The change in cloudiness that results from the increase of concentrations of atmospheric trace gases may play an important role in the climate sensitivity. Related problems such as the "greenhouse effect" have been extensively studied in the last decade (e.g., Manabe and Stouffer, 1980; Washington and Meehl, 1983; Wetherald and

Manabe, 1988). An accurate representation of clouds in these climate change studies is crucial.

Clouds are classified according to their visual appearance, their development and their altitude. The complete international classification includes dozens of cloud types. Following London (1957), clouds are divided into 6 classes: cirrus, altostratus, nimbostratus, stratus, cumulus and cumulonimbus. Stratiform clouds are produced by synoptic scale vertical air motions arising from large-scale convergence, frontal lifting, or orographic lifting of air that is statically stable. Near the ground they are also formed by radiative cooling and mixing of air masses of widely different temperatures. These clouds can extend over hundreds of kilometers in the horizontal and are usually confined to layers less than 1 km deep. Low-level stratus clouds are often capped by a temperature inversion, inhibiting further vertical growth. At the cloud tops, there is a significant radiative and evaporative cooling. Observations reveal that stratus clouds are horizontally homogeneous on large-scale but exhibit variability on a small scale. On the other hand, cumulus clouds are caused by convection in unstable air. Their horizontal and vertical extents are comparable, and the vertical extent is controlled by the depth of the unstable layer and its degree of instability. They are usually small-scale in horizontal and much larger in vertical depth compared to the stratiform clouds. Cumulus clouds have a large natural variability. Cloud properties are systematically different between land and ocean: Oceans have larger cloud cover with somewhat larger optical thicknesses and lower cloud top altitudes. The tropics are covered predominantly by high clouds, the subtropics by low clouds and midlatitudes are covered by low and middle clouds.

Most general circulation models (GCMs) today include interactive (but still highly simplified) cloudiness parameterization. GCMs are being used to predict the response of the climate to increased carbon dioxide concentrations and other perturbations. Deficiencies and uncertainties in current GCM cloudiness parameterizations are among the most serious obstacles preventing full confidence in the results of such climate forecasts (e.g., Schlesinger and Mitchell, 1987; Wetherald and Manabe, 1988). Most early GCMs included only prescribed zonally uniform clouds. Numerical experiments with these models have demonstrated that the large-scale circulation systems are indeed sensitive to the parameterized clouds (e.g., Herman et al., 1980; Meleshko and Wetherald, 1981; Shukla and Sud, 1981; Hunt, 1982; Ramanathan et al., 1983; Charlock and Ramanathan, 1985). The prediction of cloud amount, height and thickness in a numerical model presents major problems because, firstly, the formation and dissipation processes are poorly understood and, secondly, most clouds are sub-grid scale, if not horizontally, then vertically. Hence, cloud related processes have to be parameterized. Although some advances have been made in the representation of clouds in these models in the recent decade, cloudiness parameterization is still in its infancy and the relationship between clouds and other physical processes is still not very clear. Most of the existing cloudiness parameterization schemes in numerical models are diagnostic. The cloudiness is empirically estimated from large-scale variables such as relative humidity. This approach bypasses the formative and dissipative processes of clouds. In the diagnostic approach two schemes " discrete" and "continuous" are used: The discrete schemes assume a fixed cloud fraction for total cloudiness (Somerville et al., 1974; Suarez et al., 1983; Randall et al., 1989; Wetherald and Manabe, 1980, 1988), stratiform cloudiness (Gates and Schlesinger, 1977; Gordon, 1983; Ramanathan et al., 1983) or for convective cloudiness (Ramanathan et al., 1983) based on a relative humidity threshold. Among the continuous schemes both linear and nonlinear functions of relative humidity are in use. In these schemes low, middle and high stratiform cloud fractions are calculated using different relative humidity thresholds and coefficients (Slingo, 1980; Geleyn, 1981; Slingo, 1987). Besides relative humidity as a diagnostic parameter for convective cloudiness, cumulus mass flux (Slingo, 1980) and surface precipitation rate (Slingo, 1987) are also used. Restrictions on the vertical velocity or the stability parameter were also imposed in some schemes, mainly for stratocumulus clouds (Schneider et al., 1978; Slingo, 1980, 1987).

These diagnostic relations are empirical in nature and give little attention to the consistency of diagnosed cloudiness with the condensation schemes present in the model. Recently, there has been some effort to develop prognostic schemes for the representation of clouds. In these schemes cloud water content is a dynamic field predicted in the numerical model (Sundqvist, 1978, Sundqvist et al., 1989; Smith, 1990) which provides a physical link between the model's hydrological cycle, thermodynamics and cloudiness prediction. These schemes allow partial cloudiness and condensation associated with the stratiform clouds in the model grid boxes. In contrast to the diagnostic approach of cloudiness parameterization, these schemes provide cloudiness estimates consistent with the formative and dissipative processes of the clouds parameterized in the model.

Lately, some attention has been paid to validate cloudiness paramerizations. Xu and Krueger (1991) used a two-dimensional numerical cumulus ensemble model to evaluate the cloudiness parameterization using large-scale variables including relative humidity, cumulus mass flux, large-scale velocity and surface precipitation rate. They also examined the dependence of the diagnostic relation on the horizontal averaging distance. Morcrette (1991), Raustein et al., (1991) and Norquist and Yang (1992) evaluated their model generated cloudiness with satellite observations. Recently Sheu and Curry (1992) also examined various diagnostic cloudiness parameterization schemes using US Air Force three-dimensional Nephanalysis derived cloudiness over the North Atlantic region. Observational studies on the First ISCCP (International Satellite Cloud Climatology Project) Regional Experiment (FIRE) data are shedding more light on marine stratiform clouds (Paluch and Lenschow, 1991) and cirrus clouds (Starr and Wylie, 1990).

Recently, we have implemented the Sundqvist et al., (1989) condensation scheme in the Canadian Global Spectral model. This paper presents the implementation of the condensation scheme and addresses the issue of cloud cover parameterization in the scheme and its verification with the satellite observed cloud cover. The grid-scale relative humidity threshold is a critical parameter in determining the sub-grid stable condensation in the scheme. There have been some studies to relate an appropriate relative humidity threshold to the horizontal model resolution for specifying stratiform cloud cover. It is widely believed that the threshold value has to be systematically increased as horizontal resolution is increased because the stratiform clouds become more resolved at higher resolution. On the contrary, some recent studies by Kiehl and Williamson (1991) and Kristjánsson (1991) on cloud parameterization at different horizontal resolutions have shown that the cloud cover decreases systematically with increasing resolution. Kristjansson (1991) noticed in his study that even at 80% relative humidity threshold their model underestimated cloud cover at high resolution and concluded that an increase in relative humidity threshold for higher resolution will be, in fact, undesirable. This appears to break down the concept of better resolved stable clouds at higher resolution but in fact in all these studies the question of vertical resolution has been neglected. In the present study we explore the relationship between relative humidity threshold and the vertical resolution and try to answer this question. We also propose a simple vertically sub-grid stratiform cloud cover parameterization. Section 2 of the paper describes the large-scale atmospheric model used at the Canadian Meteorological Center (CMC). Section 3 contains a brief description of the condensation scheme. Section 4 discusses the data sets used in this study. Sections 5 and 6 present the numerical experiments conducted and their results and discussion. Conclusions are presented in Section 7.

2. The model

The Canadian global spectral model (Ritchie, 1991) is based on the primitive equations and the hydrostatic approximation. The model employed in this study is modified by adding a cloud water conservation equation. It uses a terrain following σ coordinate (σ = pressure/surface pressure) in the vertical. The model uses vector momentum $\boldsymbol{v}$ form of the equations of motion in horizontal and a generalized geopotential P $(=\Phi + RT^* \ln p_s$; where Φ is the geopotential height, R is the gas constant, T^* is a temperature constant and p_s is the surface pressure). The time integration is performed using a semi-Lagrangian semi-implicit approach. Using this formulation the adiabatic model equations are:

horizontal momentum equation

$$\frac{d\boldsymbol{v}}{dt} + \overline{\nabla P^t} = \overline{[-RT' \nabla \ln p_s - f\boldsymbol{k} \times \boldsymbol{v}]^s} \tag{2.1}$$

thermodynamic equation

$$\frac{\mathrm{d}T'}{\mathrm{d}t}-\frac{RT^*}{c_\mathrm{p}}\left[\frac{\mathrm{d}\ln p_\mathrm{s}}{\mathrm{d}t}+\frac{\overline{\dot\sigma}^\mathrm{t}}{\sigma}\right] = \overline{\frac{RT'}{c_\mathrm{p}}\left[\frac{\mathrm{d}\ln p_\mathrm{s}}{\mathrm{d}t}+\frac{\dot\sigma}{\sigma}\right]}^\mathrm{s}, \tag{2.2}$$

continuity equation

$$\frac{\mathrm{d}\ln p_\mathrm{s}}{\mathrm{d}t}+\overline{\nabla\cdot\boldsymbol{v}}^\mathrm{t}+\frac{\partial\overline{\dot\sigma}^\mathrm{t}}{\partial\sigma}=0, \tag{2.3}$$

moisture continuity equation

$$\frac{\mathrm{d}q}{\mathrm{d}t}=0, \tag{2.4}$$

cloud water continuity equation

$$\frac{\mathrm{d}m}{\mathrm{d}t}=0, \tag{2.5}$$

and hydrostatic relation

$$\frac{\partial P}{\partial\sigma}=-\frac{RT'}{\sigma}, \tag{2.6}$$

where the temperature T is written as sum of a constant T^* and a perturbation T', f is the Coriolis parameter, $\boldsymbol{k}$ is the vertical unit vector, c_p is the specific heat at constant pressure, $\dot\sigma$ is the vertical velocity in sigma coordinates, q is the specific humidity and m is the cloud water mixing ratio in the atmosphere.

$\overline{(\ )}^\mathrm{t}$ is a time average that is applied along the parcel trajectory to stabilize the gravity wave producing terms (semi-implicit treatment) and $\overline{(\ )}^\mathrm{s}$ is a spatial averaging (Tanguay et al., 1992) applied to the right-hand side terms along the parcel trajectory to reduce the problem related to the pressure gradient term near the mountains and to gain significant efficiency in the integration. In the 3-dimensional version of our semi-Lagrangian scheme the total time derivative $\mathrm{d}(\ )/\mathrm{d}t$ is approximated by the centred difference along the trajectory. To avoid excessive damping arising from interpolating rapidly varying fields in the vertical in the vicinity of the tropopause, a 3-dimensional scheme combining 2-dimensional semi-Lagrangian in the horizontal and non-interpolating semi-Lagrangian (Ritchie, 1986) in the vertical is used for integrating eqs. (2.1)–(2.3). A spectral method using spherical harmonics and triangular truncation in the horizontal and a finite element method (Béland and Beaudoin, 1985) in the vertical are used for the spatial discretization.

Along with the moisture continuity equation, we have also introduced an additional continuity equation for cloud-water content in the atmosphere (eq. (2.5)). The transport of cloud-water field in a large-scale model is essential to properly link the model's hydrological cycle, moist thermodynamics and cloud prediction. In addition, the radiative properties of clouds depend strongly on their water content. The presence of strong gradients and discontinuities in physical fields such as specific humidity and cloud water mixing ratio make the spectral approach and the conventional high order interpolating semi-Lagrangian schemes unattractive due to their difficulties in preserving the shape of the solutions. Various modified schemes have been developed and included in the numerical models to eliminate the overshoots and undershoots produced by these schemes. We have adapted a three dimensional extension of the Quasi-monotone semi-Lagrangain shape preserving scheme developed by Bermejo and Staniforth (1992) for the moisture and cloud water transport in the model. This scheme is a conventional semi-Lagrangian scheme coupled with a limiting procedure. The scheme is of high order in the domain of sufficiently smooth solution and is able to suppress the wiggles generated by the high-order interpolation in the neighborhood of the strong gradients of the solution.

The terms describing physical processes are computed and added after integrating the adiabatic eqs. (2.1)–(2.5) utilizing a fractional-step time integration (Yanenko, 1971) method. The following physical parameterizations are included in the model:

- relatively simple solar and terrestrial radiation schemes;
- vertical diffusion of surface fluxes based on similarity theory;
- vertical diffusion of planetary boundary layer fluxes based on turbulent kinetic energy;
- surface temperature calculated based on force-restore method;
- Sundqvist convective and stratiform condensation and cloudiness parameterization.

3. Condensation and cloudiness parameterization

In this section, we present the main features of the convective and stratiform condensation and cloudiness parameterization scheme, which is based on the method proposed by Sundqvist et al. (1989). From a modelling point of view, the problem is to relate the sub-grid scale redistribution of mass and energy by the condensation processes to the variables predicted by the model. First, we construct appropriate large-scale prognostic equations for heat, moisture and cloud-water that include the effects of the sub-grid scale clouds on the resolvable scales of motion. A unit grid volume is divided into a mean cloud and environment region and the equations for these two regions are considered separetely. The large-scale fields are defined by a grid averaging operator:

$$\bar{\alpha} = c\alpha^{c} + (1-c)\,\alpha^{d}, \tag{3.1}$$

where superscripts c and d denote 3-dimensional averages over the cloud and environment regions, c is the fractional cloud amount in the grid box and α represents any grid variable. The large-scale equations are derived by differentiating eq. (3.1) in time and grid averaging the resulting equations. The expressions for $\partial\alpha^{c}/\partial t$ and $\partial\alpha^{d}/\partial t$ are obtained by averaging the general thermodynamic, humidity and cloud water equations separately over the cloud and environmental regions. This procedure will lead to an expression for the time rate of change of grid mean fields as:

$$\begin{aligned}\frac{\partial\bar{\alpha}}{\partial t} &= -\overline{\nabla\cdot\bar{v}\bar{\alpha}} - \frac{\partial\overline{\bar{\omega}\bar{\alpha}}}{\partial p} + \bar{S} \\ &+\left[-\overline{\nabla\cdot v'\alpha'} - \frac{\partial\overline{\omega'\alpha'}}{\partial p} + \overline{\nabla\cdot\bar{v}\alpha'} + \frac{\partial\overline{\bar{\omega}\alpha'}}{\partial p}\right. \\ &\left.+\frac{\partial\overline{\alpha'}}{\partial t} + \overline{\nabla\cdot v'\bar{\alpha}} + \frac{\partial\overline{\omega'\bar{\alpha}}}{\partial p}\right],\end{aligned} \tag{3.2}$$

where α' is the generalized fluctuation from grid mean $\bar{\alpha}$ and $\bar{S}$ represents the source/sink of all cloud related micro-physical processes. Eq. (3.2) is written in p-coordinates because of its simplicity in flux form. The terms in square brackets in eq. (3.2) represent the effects of sub-grid scale fluctuations on the large-scale flow. In the present formulation, these terms are neglected in comparison to the other terms for both convective and stratiform parameterization. Although some of the eddy flux terms have been investigated in some studies for their effects on large-scale in the case of convective condensation, their effects in case of sub-grid scale stratiform condensation are unknown at present. Further research is needed in this area since stratiform clouds are comparable in area to the grid resolution of large-scale models.

The first two advective terms in (3.2) are computed using the advective scheme described in Section 2. The micro-physical term $\bar{S}$ for thermodynamic, humidity and cloud water equations can be expressed as:

thermodynamic

$$\bar{S} = c\frac{L}{c_{p}}Q^{c} - (1-c)\frac{L}{c_{p}}E^{d}_{t}, \tag{3.3}$$

moisture

$$\bar{S} = -cQ^{c} + (1-c)\,E^{d}_{t}, \tag{3.4}$$

cloud water

$$\bar{S} = c(Q^{c} - P^{c}) - (1-c)\,E^{d}_{c}, \tag{3.5}$$

where

$$E^{d}_{t} = E^{d}_{c} + E^{d}_{r}. \tag{3.6}$$

Q^{c} is the condensation rate, E^{d}_{c} is the cloud water evaporation and E^{d}_{r} is the evaporation of rain water. P^{c} is the rate of release of precipitation which includes the autoconversion rate of cloud droplets to rain drops and the accretion rate of cloud droplets by rain drops.

3.1. Convective condensation

Convective condensation (Sundqvist et al., 1989) is a modified version of the Kuo parameterization scheme (Kuo, 1965; 1974) which includes the cloud water prognostic equation, cloudiness parameterization and the parameterization of micro-physics in formation of cloud droplet, rain drops and their evaporation. The convective cloudiness is given by the expression:

$$c = \xi\tau\,\frac{(1+\Delta\sigma_{c}/0.3)}{1+2.5\xi\tau}\,(1+U), \tag{3.1.1}$$

where ξ is a proportionality factor of the Kuo scheme, τ is the characteristic time-scale (3600 s) for convection, $\Delta\sigma_c$ is the cloud thickness in σ units and U is the relative humidity. This relation for convective cloudiness ensures the increase of cloudiness as the cloud thickness and relative humidity increase and prevents c from approaching unity when ξ is large.

3.2. Stratiform condensation

Sub-grid scale stratiform condensation (Sundqvist, 1978; Sundqvist et al., 1989) is based on the following assumptions.

(1) In a statically stable grid column, if the relative humidity in a grid box exceeds a threshold value RH_c, condensation can take place in a fraction c of the box.

(2) The moisture convergence in the cloudy portion c is completely condensed.

(3) The moisture convergence in the clear portion increases the cloudiness c and the relative humidity of the cloud-free portion.

The third assumption can be expressed as:

$$(1-c)(M^d + E_t^d) = (q^c - q^d + m^c)\frac{\partial c}{\partial t} + (1-c)\frac{\partial q^d}{\partial t}, \tag{3.2.1}$$

where M^d is the convergence of vapour available for condensation and moistening which is assumed to be equal to the grid average $\bar{M}$. q^d is parameterized as a function of cloudiness as:

$$\frac{q^d}{q_s} = RH_c + c(U^c - RH_c), \tag{3.2.2}$$

and $m^c = m/c$ by definition (eq. (3.1)).

Eq. (3.2.2) along with the definition (eq. (3.1)) of mean relative humidity can be solved to provide the stratiform cloudiness as:

$$c = 1 - \left(\frac{1-U}{1-RH_c}\right)^{1/2} \tag{3.2.3}$$

where U^c has been replaced by unity and U is the grid mean relative humidity.

The expression for the rate of condensation Q^c and parameterization of other micro-physical fields (E_c, E_r and P) are obtained as described in Sundqvist et al. (1989).

4. Data

Operational humidity analyses are known to be poor over data sparse regions. For estimating cloudiness in the forecast models, good initial humidity analysis is particularly important since humidity is a crucial parameter in its parameterization. Therefore, in our simulation we decided to use a humidity analysis supplemented by satellite data. Positive impacts of humidity enhancement in cloudy regions on the spin-up time of forecasts have been shown by Turpeinen (1990), Puri and Miller (1990) and many others. Satellite derived humidity profiles using a retrieval technique based on cloud classification developed by Garand (1993) are used in the initial analysis. The scheme uses GOES visible, infrared and water vapor channels to derive dew point depression as a humidity variable at standard pressure levels. These retrievals were assimilated into the objective analysis system of CMC to provide two initial data sets valid at 0000 UTC 5 and 12 June 1991. The observed cloud top pressure and cloud fraction for the simulation periods are also derived from GOES-7 imagery. The cloud top temperature is defined by the 95th percentile in the IR histogram (5% coldest pixel) and converted to cloud top pressure using observed temperature profiles. Cloud fraction is derived using both visible (albedo) and infrared (temperature) thresholds. In daytime, the visible mode is usually chosen.

5. Experiments

5-day forecasts are performed for the two summer cases at 1.5° lat/long horizontal resolution and 21 sigma levels in vertical as given below.

0.01, 0.045, 0.09, 0.14, 0.09, 0.245, 0.304, 0.366, 0.43, 0.494, 0.558, 0.622, 0.684, 0.744, 0.8, 0.85, 0.894, 0.932, 0.964, 0.99 and 1.0.

The following experiments are conducted to evaluate the impact of cloud cover parameterization in the model and its verification with the satellite data. All the experiments use the

Sundqvist cloud water predictive condensation scheme described in Section 3.

(a) *Control.* Presently, the operational version of the CMC global model uses a non-linear diagnostic relation for total cloudiness parameterization which is expressed as:

$$c = \left(\frac{U - RH_c(\sigma)}{1 - RH_c(\sigma)} \right)^2, \tag{5.1}$$

where $RH_c(\sigma)$ is the critical relative humidity below which cloud fraction is zero. $RH_c(\sigma)$ decreases linearly from 0.98 at the surface to 0.8 at $\sigma = 0.4$. Above $\sigma = 0.4$, it is kept fixed at 0.8. This formulation does not parameterize the stratiform and convective cloudiness explicitly. In the control run the cloudiness was parameterized according to eq. (5.1).

(b) *Rht85.* Convective and stratiform cloudiness are estimated in the condensation scheme according to eqs. (3.1.1) and (3.2.3), respectively. Relative humidity threshold RH_c for the stable condensation is kept at 0.85 for this experiment.

(c) *Rhtz.* This experiment investigates the dependence of stratiform relative humidity threshold on height. Cloudiness parameterization is similar to experiment (b) except for the relative humidity threshold which is made a function of height. Positive impacts of decreasing humidity threshold with height on cloud cover estimates have been shown by many GCM studies (Slingo, 1987; Mitchell and Hahn, 1990). Since the humidity threshold, in our scheme, is also the basis of sub-grid scale stratiform condensation (Subsection 3.2), this experiment also explores the impact of RH_c decreasing with height on the latent heating and hydrological cycle of the atmosphere in addition to the cloud cover. RH_c is decreased to 0.5 for high level clouds, starting at 0.85 near the surface.

(d) *Stcvt.* This experiment is conducted to explore the importance of vertical sub-grid nature of the stratiform clouds. So far the cloud cover in a grid box was considered to be the same as the volumetric cloud fraction in the box since the Sundqvist parameterization assumed that in the presence of cloudiness (convective/stratiform) the grid box is completely filled by clouds in the vertical direction. In this experiment, we present a vertical sub-grid approach to stable clouds by making a distinction between the cloud cover and the volumetric cloud fraction in a grid box.

We treat the grid-scale relative humidity as a 3-dimensional area average over the grid cells and use the sub-grid stable condensation scheme same as before to provide a volumetric cloud fraction cf (previously termed as c) in the 3-d grid boxes. The volumetric cloud fraction cf is estimated by the expression (3.2.3). Realizing the fact that stratiform clouds are vertically thin, the volumetric cloud fraction cf is assumed to fill a larger horizontal area of the grid boxes which separates the definition of cloud cover from the cloud fraction. The 2-dimensional stratiform cloud cover (c) in a grid cell is assumed to be a linear function of cf as defined below:

Ocean

$$\begin{aligned} c &= 2.3\,cf && [0 \leqslant cf < 0.3] \\ c &= 0.25 + 1.5\,cf && [0.3 \leqslant cf < 0.5] \\ c &= 1 && [cf \geqslant 0.5] \end{aligned} \tag{5.2}$$

Land

$$\begin{aligned} c &= 1.4\,cf && [0 \leqslant cf < 0.7] \\ c &= 1 && [cf \geqslant 0.7]. \end{aligned} \tag{5.3}$$

Due to the differences between land and ocean surfaces such as topographical variations over land, relatively flat ocean surface and the differences between their heat capacities and albedo, the cloud geometry and other properties are systematically different over land and ocean. Observations reveal that oceanic clouds are more extensive, thinner and have lower cloud top altitudes. The presence of marine stratiform decks is a common phenomenon during summer time. To account for these differences in our experiment we made the distinction (5.2, 5.3) between the stratiform cloud cover parameterization over ocean and land. This need is also pointed out by the zonal diagnostics of the predicted cloud cover performed separately over the two regimes (Fig. 2, discussed in Section 6).

The subdivisions in eqs. (5.2) and (5.3) reflect the varying rate of vertical growth of a stratiform cloud in its various stages of formation. This division was guided by the satellite observed cloud cover data.

It is quite conceivable that the actual extent of the horizontal cloud cover will depend on many more factors, such as the cloud type, cloud stage (formative/dissipative), stability, surface type and the height of the cloud. As a first step, we have only used the volumetric cloud fraction to define the stratiform cloud cover. The total cloud cover is calculated by combining the horizontally sub-grid convective cloud cover and vertically sub-grid stratiform cloud cover.

(e) *Rhtzv.* Combined effects of height dependant relative humidity threshold (exp. (c)) and vertically sub-grid stable clouds (exp. (d)) are examined in this experiment.

(f) *Rht1.* The relative humidity threshold is set to one; therefore the stratiform condensation scheme is no longer sub-grid scale but it only condenses the supersaturation.

6. Results and discussion

The total cloud cover in a grid column is computed by the assumption of random/maximum overlapping of the individual levels in the column. Figs. 1(a–e) compare the simulated total cloud cover from different experiments with the observed cloud cover over a region extending from 50°–155° W and 45° S–60° N. Although our simulations are global forecasts, we particularly examined the cloud cover in this region because of the availability of GOES derived observed data for quantitative analysis of the simulation. The domain makes possible the examination of variety of cloud cover over continents, ocean, tropics, sub-tropics and midlatitudes. Here, only the 24-h forecast cloudiness is compared with the observed data to make a quantitative comparison since poor prediction of relative humidity in the large-scale models makes it very difficult to verify cloud fields on point by point basis for longer forecasts. Fig. 1a is the satellite derived cloud cover, where the white portions represent overcast sky. The ITCZ (Inter Tropical Convergence Zone) north of the equator is very clearly defined by a band of cloudiness. Extensive overcast regions are present over the oceans. The average total cloud cover of the domain is 65.5%. When compared with the cloudiness simulated by the control run (Fig. 1b) it is evident that the simulated cloud cover is underpredicted particularly over the ocean. The ITCZ is almost missing except for the high level cloudiness associated with Cbs. The reason is that the relative humidity based diagnostic relation (eq. (5.1)) is incapable of providing the convective cloudiness. The cloud free region over the gulf of Mexico is very well simulated. Fig. 1c shows the cloudiness simulated by the condensation scheme in exp. (b). It is clearly seen that in this simulation the ITCZ is better resolved and there is in general a higher amount of cloudiness present. This simulation illustrates the advantage of using a sub-grid scale condensation scheme for convective and stratiform clouds which includes the parameterization of cloudiness. Although the cloud cover is still underpredicted there is an increase in cloudiness over the ocean. Near the surface there is turbulent mixing which gives rise to a mixed layer therefore we expect the condensation to take place at a relatively high RH_c. As we move to the higher levels the atmospheric stability increases and therefore the RH_c is expected to be lower. Also, generally the models have much lower resolution for the higher levels compared to the lower levels which further makes it important to lower the threshold with height. In the exp. (c) the relative humidity threshold was decreased with height. Fig. 1d shows the cloud cover from this experiment. Comparison of this with Fig. 1c reveals a systematic increase in the simulated cloud cover. The cloud cover over land is well predicted but over the ocean it is still under-estimated. It can be seen that in all three simulations the spatial distribution of cloud cover is well predicted but the amount is under-estimated and the discrepancy is more over the ocean. Next experiment (d) was designed to explore the importance of vertically sub-grid stratiform clouds. Fig. 1e depicts the cloud cover estimated by a combination of vertically sub-grid stratiform clouds and RH_c decreasing with height (exp. (e)). There is a substantial increase in the cloud cover over the ocean and it compares well with the observation.

We also compared the observed and simulated cloud top pressures. The comparison revealed that there are more middle and low level clouds present in the observed heights compared to the simulation. Particularly West of the continents over the ocean there are much less middle and low level clouds simulated but this deficiency is alleviated when the stratiform clouds were considered vertically sub-grid.

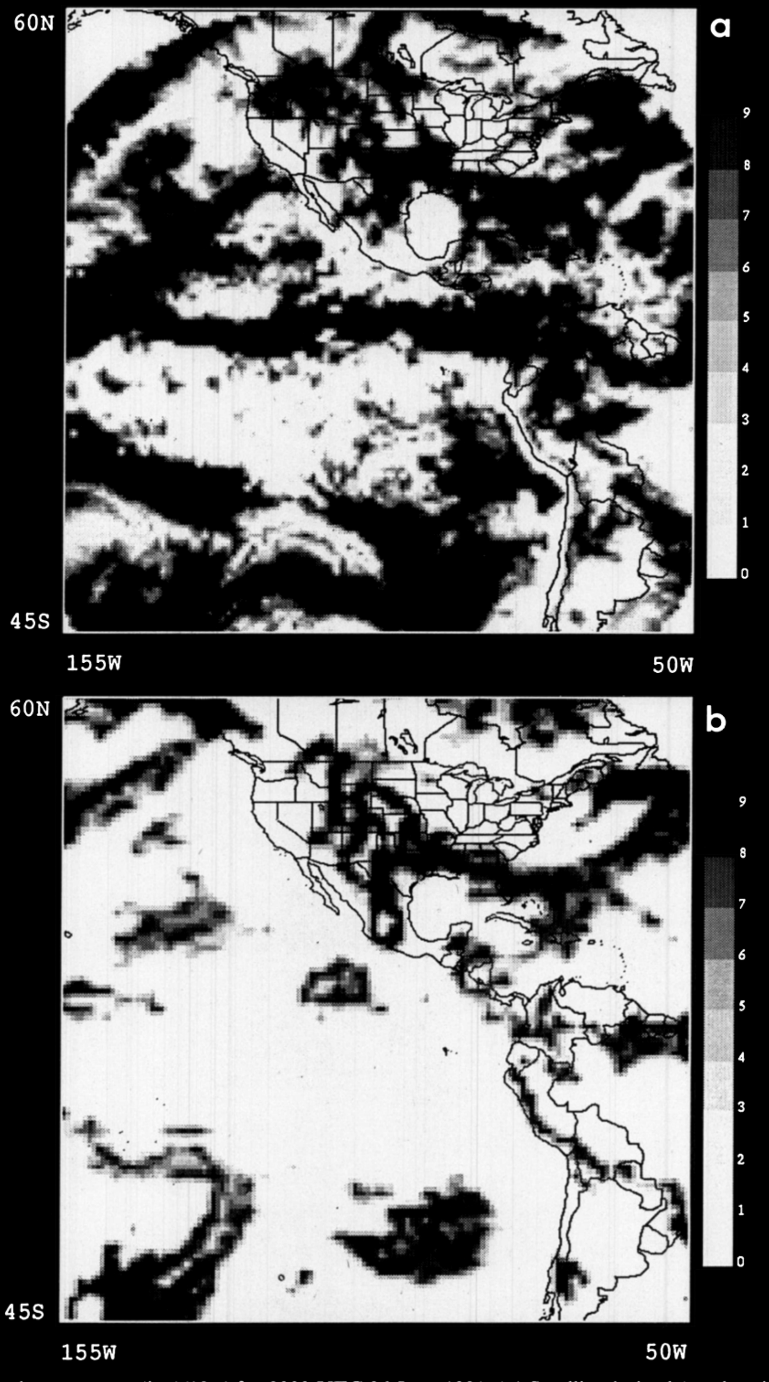

Fig. 1. Total cloud cover maps (in 1/10 s) for 0000 UTC 06 June 1991. (a) Satellite derived (no data in NW and NE corners); (b) model simulated using old cloudiness parameterization (Control); (c) model simulated using Sundqvist condensation scheme with $RH_c = 0.85$ (Rht85); (d) same as Fig. 1c but for RH_c decreasing with height (Rhtz) and (e) same as Fig. 1d but for vertical sub-grid stratiform clouds (Rhtzv).

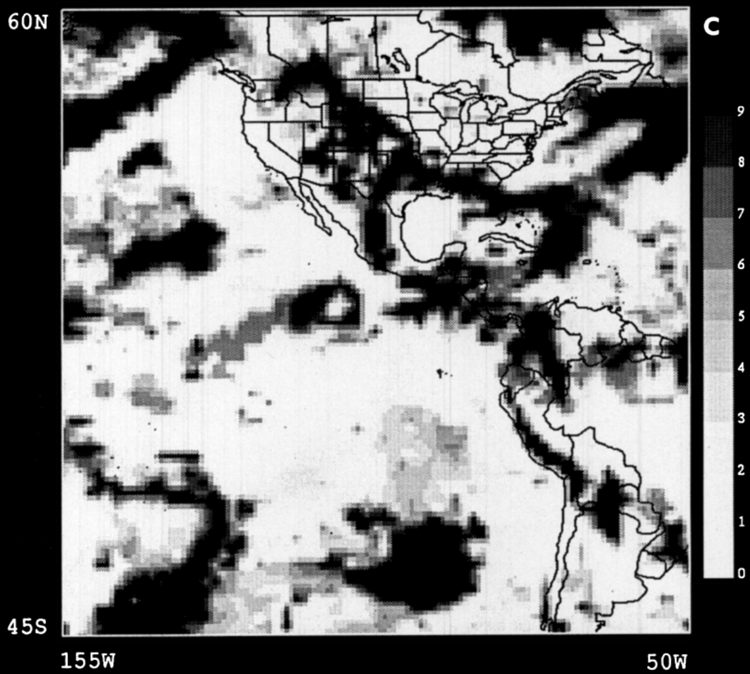

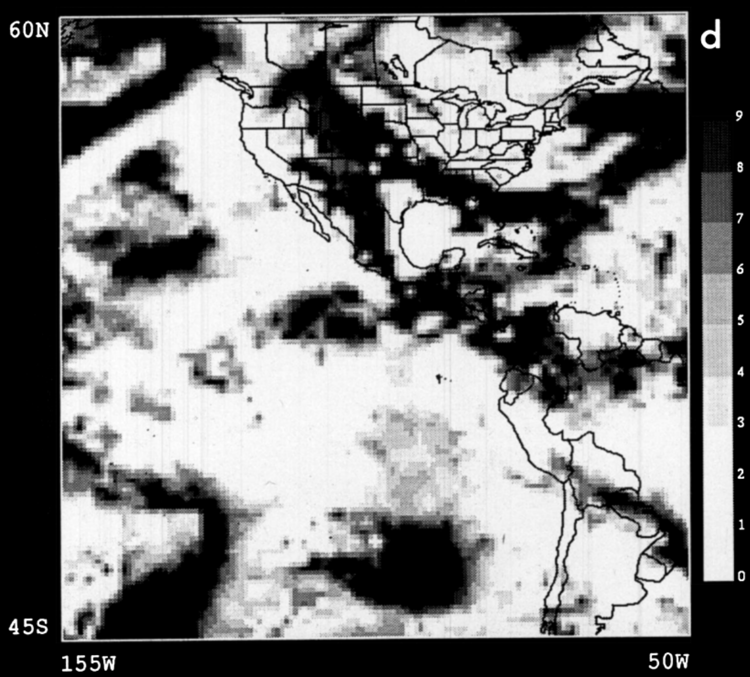

Fig. 1 (cont'd).

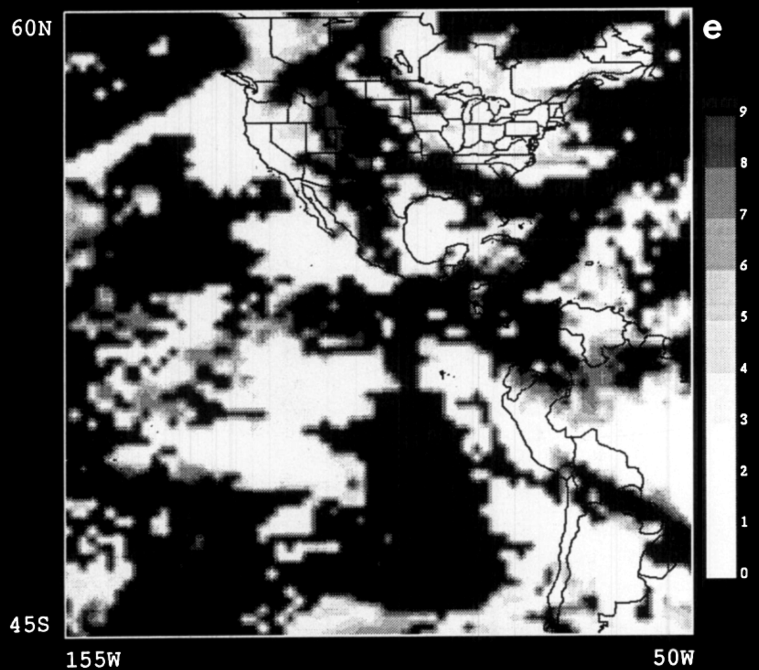

Fig. 1 (cont'd).

In order to examine the cloud cover differences over land and ocean zonal diagnostics are performed separately over the two regions. Figs. 2a, b are the observed and predicted (exp. (c)) zonal mean cloud cover over ocean and land for the same domain as in Fig. 1. The simulated maxima and minima are well correlated to the observed structure over ocean as well as land but the simulated cloud amount is much lower over the ocean as compared to the observed. We found that the main reason of less cloudiness over ocean is due to neglecting the presence of vertically thin stratus or stratocumulus clouds over the ocean. Particularly over the summer hemisphere between 20° and 40° latitude thin stratiform clouds are commonly known to form in response to strong subsidence generated by the subtropical high over a relatively cold upwelling ocean. Thin layers of marine stratiform decks below the inversion in the planetary boundary layer are known to play an important role in the global radiation budget, and consequently the earth's climate. Recent observations with the FIRE experiments have revealed that these stratus layers start as thin and rather homogeneous layers which later grow and become patchy. In the next Figs. 3a, b total zonal mean cloud covers are compared between different experiments and the observed cloudiness. The control run is seen to produce a much lower cloud cover than the observed one. The next two curves show the predicted cloud cover using relative humidity thresholds of 0.85 and 1 for stratiform clouds. Fig. 3b compares the cloud cover from exp. (b) (RH_c equal to 0.85), exp. (c) (RH_c decreasing with height) and exp. (e) (vertical sub-grid stratiform clouds and RH_c decreasing with height) with the observed cloudiness. It is clearly seen that zonal mean cloud cover simulated by the experiment using vertically sub-grid stable clouds is remarkably close to the observed curve. The cloud cover in the ITCZ is still under-estimated. A possible explanation for this discrepancy is the lack of parameterization for shallow convective clouds. Further, the ITCZ is seen to be broader in simulation, compared to the sharp peak in the observed curve. Lower resolution of the model simulation over the tropics can lead to this broadening of the cloudy regions. Similar results were obtained for another simulation for which the average cloud cover over land, ocean and combined are presented in Table 1b.

Figs. 4a–c compare the mean cloud cover for different simulations with the GOES derived cloud cover averaged over all grid points, land points and ocean points respectively. The values of mean

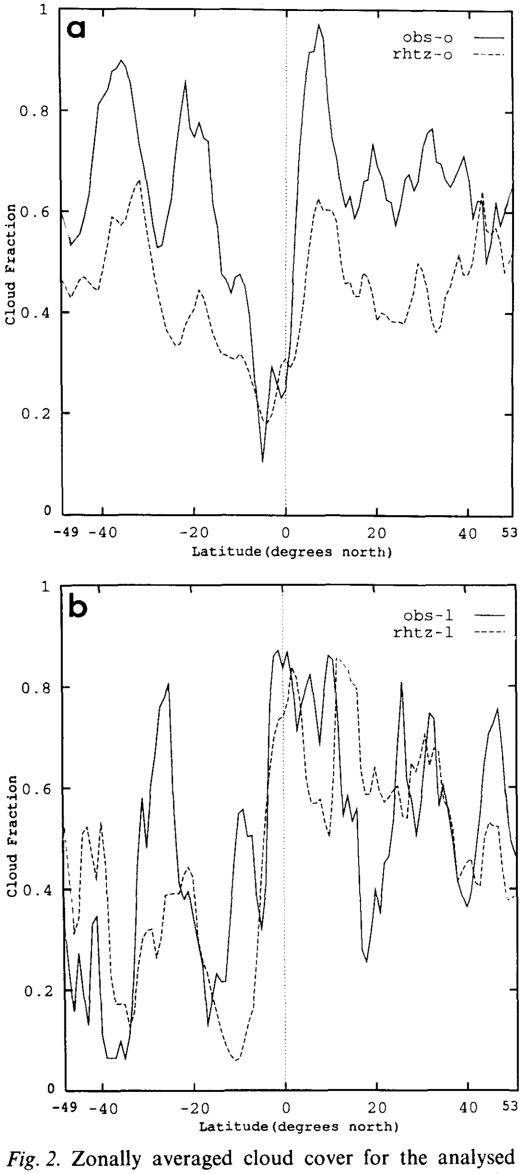

Fig. 2. Zonally averaged cloud cover for the analysed domain valid at 0000 UTC 6 June 1991 as observed by satellite (solid line) and as simulated by the experiment Rhtz (dashed line) for (a) ocean and (b) land.

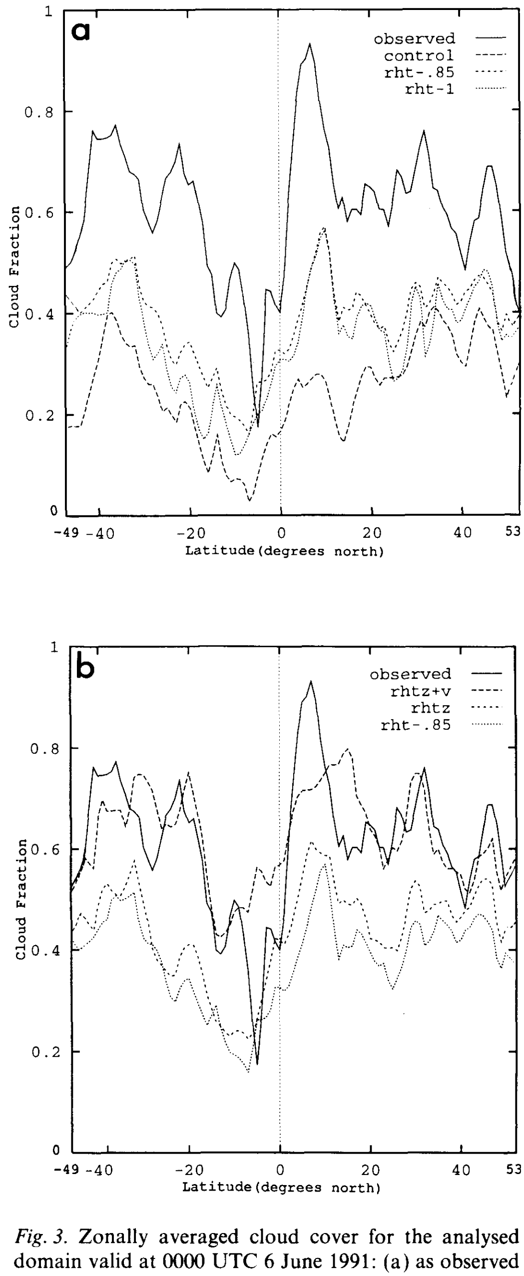

Fig. 3. Zonally averaged cloud cover for the analysed domain valid at 0000 UTC 6 June 1991: (a) as observed by satellite (solid line), as simulated by control run (dashed line), as simulated by the experiment Rht85 (short dashed line) and as simulated by the experiment Rht1 (dotted line); (b) as observed by satellite (solid line), as simulated by the experiment Rhtzv (dashed line), as simulated by the experiment Rhtz (short dashed line) and as simulated by the experiment Rht85 (dotted line).

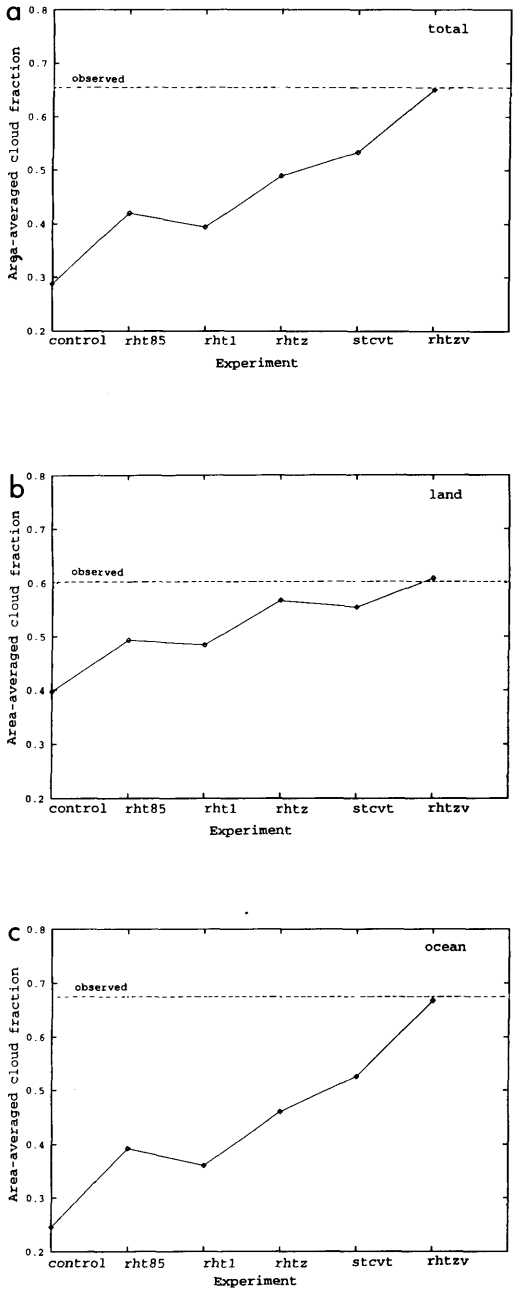

Fig. 4. Area-averaged cloud cover for the analysed domain for 0000 UTC 6 June 1991 as observed by the satellite (dashed line) and model simulated by experiments control, Rht85, Rht1, Rhtz, Stcvt and Rhtzv (solid line) for (a) all grid points, (b) only land points and (c) only ocean points included.

cloud cover are also given in Table 1a. Except for exp. (e), all other simulations predict a much lower cloud cover over ocean than over land. The observed mean cloud cover is larger over ocean (0.675) compared to land (0.602) which is in quite good agreement with the cloud cover simulated by exp. (e). An important point to note here is that the difference in mean cloudiness between experiments Rht85 and Rht1 is only 2.6% whereas it is about 7% between experiments Rht85 and Rhtz and 11% between experiments Rht85 and Stcvt. These differences illustrate that the stratiform clouds depend on vertical resolution more crucially than on horizontal resolution and they are more often vertically sub-grid.

Figs. 5a–f show the frequency distribution of fractional cloudiness for the simulation experiments and for the satellite derived cloud cover. It is noticed in Fig. 1a that the satellite cloud cover has very sharp boundaries, the regions of cloudiness lower than 90% are very narrow, which is further confirmed in Fig. 5a where 50% grid

Table 1a. *Area-averaged cloud cover for the satellite analysed domain as observed by the satellite and simulated by different experiments: valid at 0000 UTC 06 June 1991 (Case 1)*

	Mean cloud cover		
Experiment	total	land	ocean
observed	0.655	0.602	0.675
control	0.288	0.397	0.246
Rht85	0.420	0.493	0.392
Rht1	0.394	0.484	0.360
Rhtz	0.489	0.567	0.460
Stcvt	0.533	0.554	0.525
Rhtzv	0.651	0.608	0.668

Table 1b. *Area-averaged cloud cover for the satellite analysed domain as observed by the satellite and simulated by different experiments: valid at 0000 UTC 13 June 1991 (Case 2)*

	Mean cloud cover		
Experiment	total	land	ocean
observed	0.689	0.608	0.720
Rht85	0.444	0.533	0.411
Rhtz	0.527	0.569	0.510
Rhtzv	0.723	0.612	0.765

points are between 0.9 to 1 cloud cover and all other cloud fractions are below 10%. Once again the frequency distribution for experiment Rhtzv is very similar to the observed pattern and all other experiments show much higher percentage of fractional cloudiness less than 0.9 compared to observed. Similar features were noted by Raustein et al. (1991) in their study of comparison between simulated cloudiness and clouds objectively derived from satellite data.

The next few figures examine the impact of cloudiness parameterization on the model forecast.

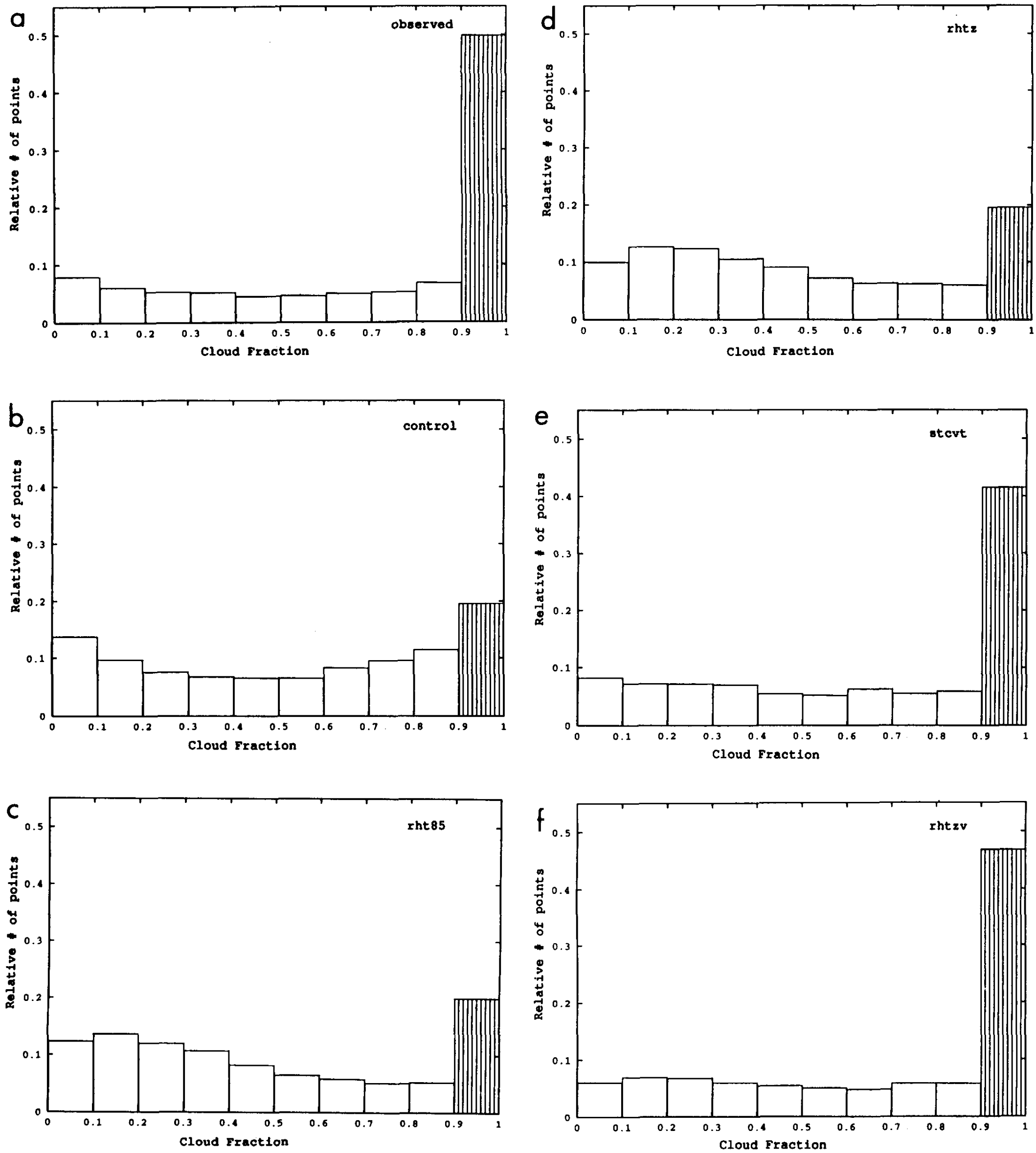

Fig. 5. Frequency distribution of cloud cover for the domain analysed by satellite for 0000 UTC 6 June 1991: (a) as observed by the satellite and (b)–(f) as simulated by the model for control run and for the experiments Rht85, Rhtz, Stcvt and Rhtzv respectively.

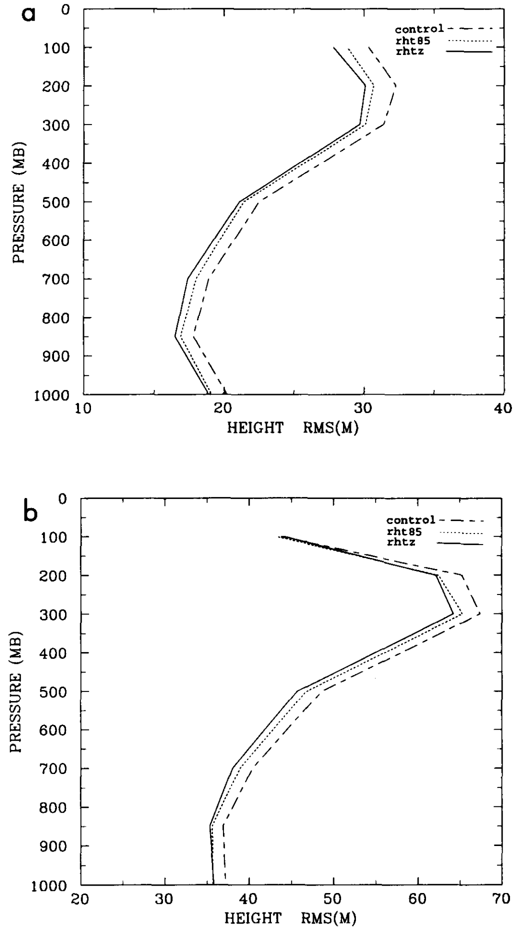

Fig. 6. Unbiased root mean square errors over the Northern Hemisphere for the model simulated height fields for the experiments control (dashed line), Rht85 (dotted line) and Rhtz (solid line) at the end of (a) day 2 and (b) day 5.

Figs. 6a, b are unbiased root mean square errors (r.m.s.) over the northen hemisphere at different pressure levels in the height forecasts at the end of 2 and 5 days. There is a reduction in r.m.s. errors when cloudiness was parameterized using the Sundqvist condensation scheme (Rht85) and a further reduction in errors was achieved when the RH_c was made a function of height (Rhtz). To explore the main source of improvement in the forecast between control and Rht85 another experiment was conducted where convective cloudiness was eliminated from the parameterization in the experiment Rht85. Fig. 7 shows 2 day r.m.s. errors from this experiment along with the total cloud cover interaction (Rht85). The differences reveal that the major improvements in the forecast Rht85 seen in Figs. 6a, b come from the radiative impact of the convective cloud cover parameterized in case of Rht85. The errors in mean height forecasts at different pressure levels for these simulations are shown in Figs. 8a, b. A major improvement in mean height prediction is noticed for the experiment Rhtz at all levels. This bias correction is mainly due to increased latent heating and the radiative effects of increased cloudiness in middle and high levels when RH_c was decreased with height. Figs. 9a–d show 24-h averages of global mean surface evaporation and precipitation rates. There is almost no spin-up in the model simulation, this is due to the enhanced initial moisture analysis using satellite data. Surface evaporation rate is very high in the control experiment due to high surface temperatures. At the end of 5 days, there is a residual of about 0.4 mm/day. For the next two experiments where RH_c is 0.85 and 1, respectively, the evaporation rate is lower but the precipitation also dropped. When the RH_c is decreased with height thereby producing more middle and high level clouds, Fig. 9d shows that by the end of 5 days a good hydrological balance is achieved in the model. The residual is close to zero

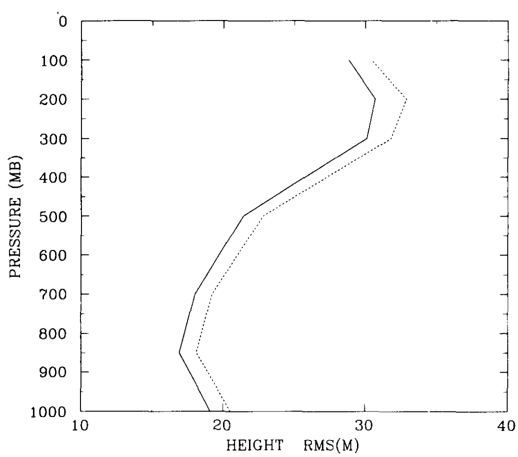

Fig. 7. Unbiased root mean square errors over the Northern Hemisphere for the model simulated height fields for experiment Rht85, where both convective and stratiform cloudiness interact with the radiation (solid line) and another experiment where only stratiform cloudiness is interactive with the radiation (dotted line).

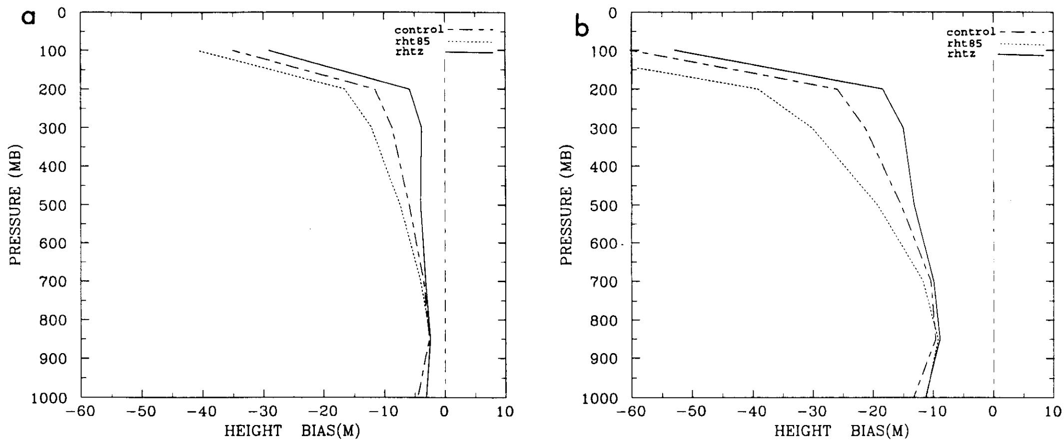

Fig. 8. Bias errors over the Northern Hemisphere for the model simulated height fields for the experiments control (dashed line), Rht85 (dotted line) and Rhtz (solid line) at the end of (a) day 2 and (b) day 5.

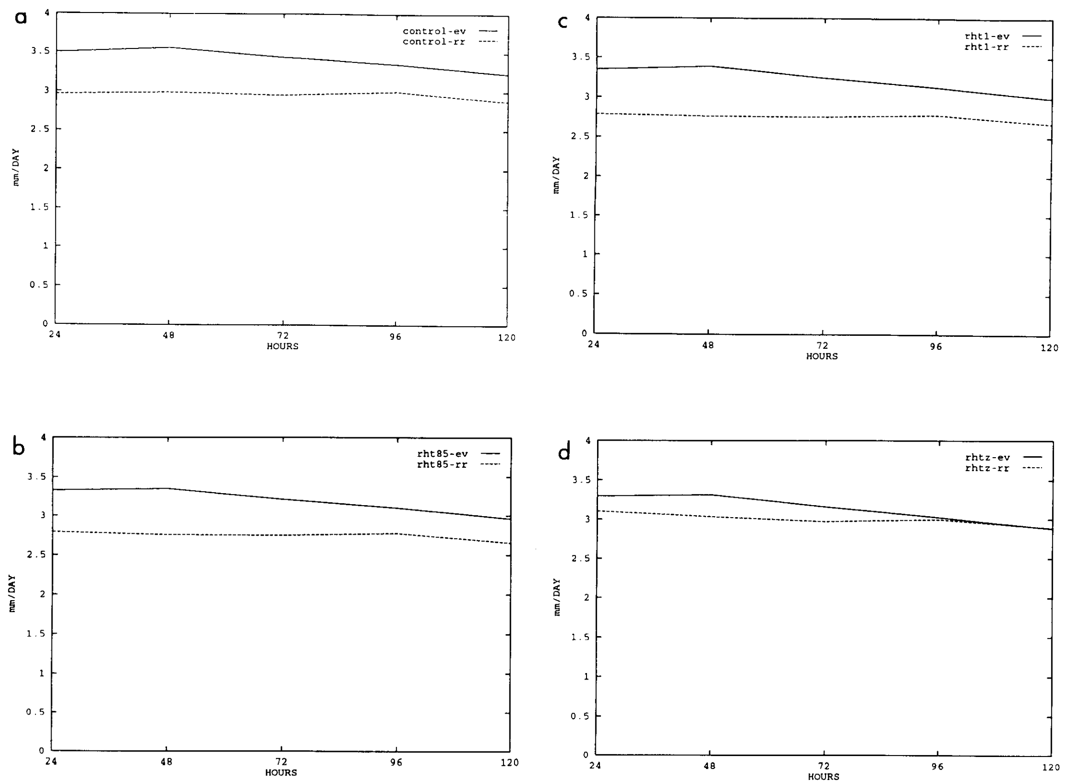

Fig. 9. Model simulated daily averaged global mean evaporation (solid line) and precipitation (dashed line) rates in mm/day for experiments (a) control, (b) Rht85, (c) Rht1 and (d) Rhtz.

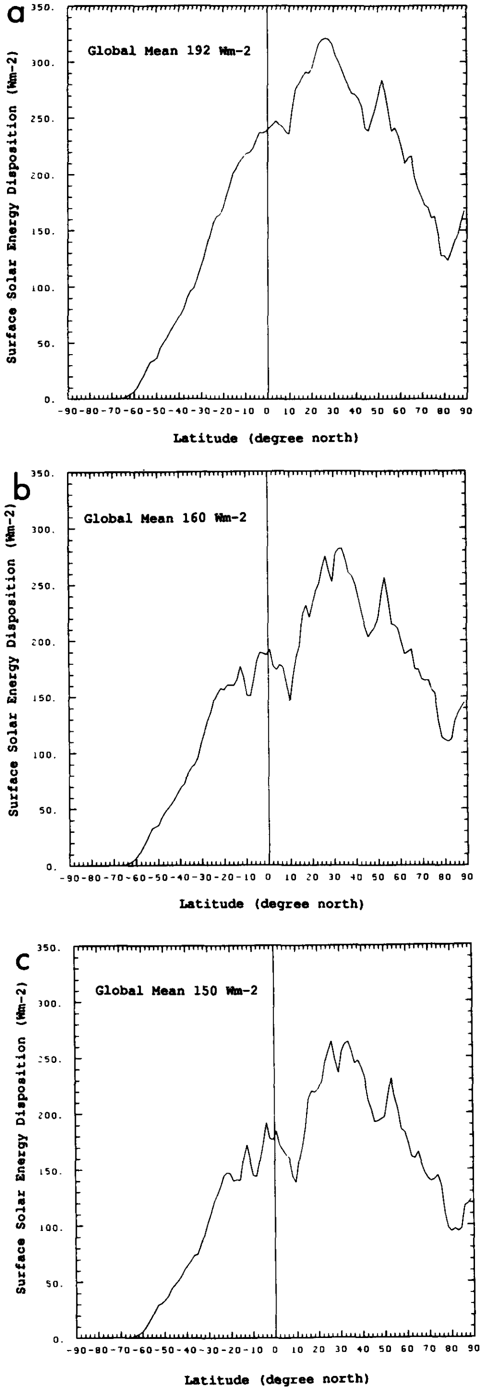

Fig. 10. 24-h average model simulated zonal mean solar energy disposition (W/m^2) at the surface for the experiments (a) control, (b) Rht85 and (c) Rhtz.

and the global mean rate of precipitation is about 2.9 mm/day which is close to the climatological mean 3.1 mm/day as estimated by Ramanathan et al. (1989). Changing RH_c from 0.85 to 1 has very little impact on the water budget as seen in Figs. 9b, c. Figs. 10a–c show global zonal averages of solar energy disposition at the earth surface in the control, Rht85 and Rhtz simulations. It is evident from the figures that the solar disposition at the surface is very high for the control run and the minimum associated with the ITCZ (north of equator) is not well defined. This is mainly due to the lack of parameterized clouds which leads to less solar absorption in the atmosphere. According to Li and Leighton (1992) the climatological estimate based on five years of ERBE data the global mean solar energy disposition at the surface is 156.9 W/m^2. It is 192 W/m^2 for the control simulation which is much higher and it is 160 and 150 W/m^2 for the experiments Rht85 and Rhtz which are in good agreement with the climatology.

7. Conclusion

In this paper, we have demonstrated the importance of parameterizing cloudiness as a product of condensation processes parameterized in a large-scale atmospheric model. The main focus of this study has been to verify the total cloud cover predicted by the scheme and to understand the sub-grid scale of the stratiform clouds defined by the relative humidity threshold. The main conclusions of the study are the following.

(1) The parameterization of convective cloudiness has an important impact on the atmospheric dynamics through its radiative interactions. A significant improvement upto five days is achieved in height forecasts.

(2) Quite accurate estimates of cloud cover can be obtained by considering the stratiform clouds as vertically sub-grid. The relative humidity threshold is a strong function of the vertical resolution of the model rather than the horizontal resolution. An increase in horizontal resolution while keeping the vertical resolution constant does not imply an increase in the relative humidity threshold as stratiform clouds are not horizontally sub-grid at most of the horizontal resolutions of the models. Recent observational studies

from FIRE (Starr and Wylie, 1990; Paluch and Lenschow, 1991) reveal that a vertical resolution of the order of 0.5 km is required to adequately resolve the cirrus clouds and much higher resolution will be required for implementation of a physically-based parameterization for stratus clouds as they can start as very thin layers. Therefore it is necessary to use a stratiform relative humidity threshold lower than unity even for very high resolution mesoscale models since the model predicted relative humidity represents the three-dimensional average in the grid boxes and the models are generally much coarser in vertical than the resolution required for stratiform clouds.

(3) We have also shown that the stratiform cloudiness computed by the Sundqvist et al. (1989) condensation scheme can be treated as a volumetric cloud fraction present in the grid boxes and a simple parameterization can be used to determine the sub-grid scale 2-dimensional cloud cover. The need for parameterizing stable clouds over ocean and land separately is also identified and included in the scheme.

(4) An improvement in cloud cover estimates and global hydrological and radiative balance is found when the relative humidity threshold is decreased with height. This strong dependence with height is related to the vertical structure of the atmosphere and the vertical discritization of the model. This result was also noted by others in GCM (Slingo, 1987; Mitchell and Hahn, 1990) studies and recently by Xu and Krueger (1991) in a study on evaluation of cloudiness parameterization schemes and by Sheu and Curry (1992) in their studies on North Atlantic clouds.

Although quite good estimates of cloud cover are obtained by a simple parameterization of stratiform cloudiness, further research on including the information about the cloud type, cloud stage, cloud height above the ground and stability of the atmosphere, will be useful.

8. Acknowledgments

The author is grateful to Professor Hilding Sundqvist for providing a version of his cloud parameterization scheme, to Dr. Claude Girard for his valuable advise and discussions, and to Dr. P. Dastoor for helpful discussions and editorial assistance in preparing the manuscript. Dr. L. Garand, Dr. J. Pudykiewicz and Dr. R. Benoit are thanked for their careful review of the manuscript. Dr. L. Garand is also thanked for providing his satellite-based analyses. The manuscript benefited from constructive comments by the two anonymous reviewers. The research was supported by the Natural Sciences and Engineering Research Council of Canada through a visiting fellowship for Canadian Government Laboratories.

REFERENCES

Albrecht, B. and Cox, S. K. 1975. The large-scale response of the tropical atmosphere to cloud modulated infrared heating. *J. Atmos. Sci.* **32**, 16–24.

Béland, M. and Beaudoin, C. 1985. A global spectral model with a finite element formulation for the vertical discretization: adiabatic formulation. *Mon. Wea. Rev.* **113**, 1910–1919.

Bermejo, R. and Staniforth, A. 1992. The conversion of semi-Lagrangian advection schemes to quasi-monotone schemes. *Mon. Wea. Rev.* **120**, 2622–2632.

Charlock, T. P. and Ramanathan, V. 1985. The albedo field and cloud radiative forcing produced by a general circulation model with internally generated cloud optics. *J. Atmos. Sci.* **42**, 1408–1429.

Garand, L. 1993. A pattern recognition technique for retrieving humidity profiles from meteosat or GOES imagery. *J. Appl. Meteor.*, in press.

Gates, W. J. and Schlesinger, M. E. 1977. Numerical simulation of the January and July global climate with a two-level atmospheric model. *J. Atmos. Sci.* **34**, 36–76.

Geleyn, J.-F. 1981. Some diagnostics of the cloud-radiation interaction in the ECMWF forecasting model. *Workshop on radiation and cloud-radiation interaction in numerical modeling*. Reading, UK, ECMWF, 135–162.

Gordon, H. B. 1983. Synoptic cloud variations in a low resolution spectral atmospheric model. *J. Geophys. Res.* **88**, 6563–6575.

Herman, G., Wu, M.-L. and Johnson, W. T. 1980. The effects of clouds on the earth's solar and infrared radiation budgets. *J. Atmos. Sci.* **37**, 1251–1261.

Hunt, G. E. 1982. On the sensitivity of a general circulation model climatology to changes in cloud structure and radiative properties. *Tellus* **34**, 29–38.

Kiehl, J. T. and Williamson, D. L. 1991. Dependence of cloud amount on horizontal resolution in the NCAR Community Climate Model. *J. Geophys. Res.* **96**, 10955–10980.

Kristjánsson, J. E. 1991. Cloud parameterization at different horizontal resolutions. *Quart. J. Roy. Meteor. Soc.* **117**, 1255–1280.

Kuo, H. L. 1965. On formation and intensification of tropical cyclones through latent heat release by cumulus convection. *J. Atmos. Sci.* **22**, 40–63.

Kuo, H. L. 1974. Further studies of the parameterization of the influence of cumulus convection on large scale flow. *J. Atmos. Sci.* **31**, 1232–1240.

Li, Z. and Leighton, H. G. 1992. Global climatologies of solar radiation budgets at the surface and in the atmosphere from 5 years of ERBE data. *J. Geophys. Res.*, in press.

London, J. 1957. *A study of the atmospheric heat balance.* New York University, 75 pp.

Manabe, S. and Stouffer, R. J. 1980. Sensitivitity of a global climate model to an increase of CO_2 concentration in the atmosphere. *J. Geophys. Res.* **85**, 5529–5554.

Meleshko, V. P. and Wetherald, R. T. 1981. The effect of a geographical cloud distribution on climate: A numerical experiment with an atmospheric general circulation model. *J. Geophys. Res.* **86**, 11995–12014.

Mitchell, K. E. and Hahn, D. C. 1990. Objective development of diagnostic cloud forecast schemes in global and regional models. *AMS Report of 7th Conference on Atmospheric radiation.* J138–J145.

Morcrette, J.-J. 1991. Evaluation of model-generated cloudiness: Satellite-observed and model-generated diurnal variability of brightness temperature. *Mon. Wea. Rev.* **119**, 1205–1224.

Norquist, D. C. and Yang, C. 1992. Comparing model-produced convective cloudiness with observations. *Mon. Wea. Rev.* **120**, 770–786.

Paluch, I. R. and Lenschow, D. H. 1991. Stratiform cloud formation in the marine boundary layer. *J. Atmos. Sci.* **48**, 2141–2158.

Puri, K. and Miller, M. J. 1990. The use of satellite data in the specification of convective heating for diabatic initialization and moisture adjustment in numerical weather prediction models. *Mon. Wea. Rev.* **118**, 67–93.

Ramanathan, V. 1987. The role of Earth radiation budget studies in climate and general circulation research. *J. Geophys. Res.* **92**, 4075–4095.

Ramanathan, V., Barkstrom, B. R. and Harrison, E. F. 1989. Climate and the earth's radiation budget. *Phys. Today* **42**, 22–32.

Ramanathan, V., Pitcher, E. J., Malone, R. C. and Blackmon, M. L. 1983. The response of spectral general circulation model to refinements in radiative processes. *J. Atmos. Sci.* **40**, 605–630.

Randall, D. A., Harshvardhan, Dazlich, D. A. and Corsetti, T. G. 1989. Interactions among radiation, convection, and large-scale dynamics in a general circulation model. *J. Atmos. Sci.* **46**, 1943–1970.

Raustein, E., Sundqvist, H. and Katsaros, K. B. 1991. Quantitative comparison between simulated cloudiness and clouds objectively derived from satellite data. *Tellus* **43A**, 306–320.

Ritchie, H. 1986. Eliminating the interpolation associated with the semi-Lagrangian scheme. *Mon. Wea. Rev.* **114**, 135–146.

Ritchie, H. 1991. Application of the semi-Lagrangian method to a multilevel spectral primitive-equation model. *Quart. J. Roy. Meteor. Soc.* **117**, 91–106.

Schlesinger, M. E. and Mitchell, J. F. B. 1987. Climate model simulations of the equilibrium climatic response to increased carbon dioxide. *Rev. Geophys.* **25**, 760–798.

Schneider, S., Washington, W. M. and Chervin, R. M. 1978. Cloudiness as a climatic feedback mechanism: effects on cloud amount of prescribed global and regional surface temperature changes in the NCAR-GCM. *J. Atmos. Sci.* **35**, 2207–2221.

Sheu, R.-S. and Curry, J. A. 1992. Interactions between North Atlantic clouds and the large-scale environment. *Mon. Wea. Rev.* **120**, 261–279.

Shukla, J. and Sud, Y. 1981. Effect of cloud-radiation feedback on the climate of a general circulation model. *J. Atmos. Sci.* **38**, 2337–2353.

Slingo, J. M. 1980. A cloud parameterization scheme derived from GATE data for use with a numerical model. *Quart. J. Roy. Meteor. Soc.* **106**, 747–770.

Slingo, J. M. 1987. The development and verification of a cloud prediction scheme for the ECMWF model. *Quart. J. Roy. Meteor. Soc.* **113**, 899–927.

Smith, R. N. B. 1990. A scheme for predicting layer clouds and their water content in a general circulation model. *Quart. J. Roy. Meteor. Soc.* **116**, 435–460.

Somerville, R. C. J., Stone, P. H., Halem, M., Hansen, J., Hogan, J. S., Druyan, L. M., Russell, G., Lucis, A., Quirk, W. J. and Tenenbaum, J. T. 1974. The GISS model of the global atmosphere. *J. Atmos. Sci.* **31**, 84–117.

Starr, D. O'C. and Wylie, D. P. 1990. The 27–28 October 1986 FIRE cirrus case study: Meteorology and clouds. *Mon. Wea. Rev.* **118**, 2259–2287.

Stephens, G. L. and Webster, P. J. 1979. Sensitivity of radiative forcing to variable cloud and moisture. *J. Atmos. Sci.* **36**, 1542–1556.

Suarez, M. J., Arakawa, A. and Randall, D. A. 1983. The parameterization of the planetary boundary layer in the UCLA general circulation model: formulation and results. *Mon. Wea. Rev.* **113**, 2224–2243.

Sundqvist, H. 1978. A parameterization scheme for non-convective condensation including prediction of cloud water content. *Quart. J. Roy. Meteor. Soc.* **104**, 677–690.

Sundqvist, H., Berge, E. and Kristjansson, J. E. 1989. Condensation and cloud parameterization studies with a mesoscale Numerical Weather Prediction model. *Mon. Wea. Rev.* **117**, 1641–1657.

Tanguay, M., Yakimiw, E., Ritchie, H. and Robert, A.

1992. Advantages of spatial averaging in semi-implicit semi-Lagrangian schemes. *Mon. Wea. Rev.* **120**, 113–123.

Turpeinen, O. 1990. Diabatic initialization of the Canadian Regional Finite-Element (RFE) model using satellite data. Part II: Sensitivity to humidity enhancement, latent-heating profiles and rain rates. *Mon. Wea. Rev.* **118**, 1396–1407.

Washington, W. M. and Meehl, G. A. 1983. General circulation model experiments on the climatic effects due to a doubling and quadrupling of carbon dioxide concentration. *J. Geophys. Res.* **88**, 6600–6610.

Webster, P. J. and Stephens, G. L. 1980. Tropical upper tropospheric extended clouds: Inferences from Winter MONEX. *J. Atmos. Sci.* **37**, 1521–1541.

Wetherald, R. T. and Manabe, S. 1980. Cloud cover and climate sensitivity. *J. Atmos. Sci.* **37**, 1485–1510.

Wetherald, R. T. and Manabe, S. 1988. Cloud feedback processes in a general circulation model. *J. Atmos. Sci.* **45**, 1397–1415.

Xu, K. M. and Krueger, S. K. 1991. Evaluation of cloudiness parameterizations using a cumulus ensemble model. *Mon. Wea. Rev.* **119**, 342–367.

Yanenko, N. N. 1971. *The method of fractional steps.* Springer, New York.